Supporting Information

Hierarchical Carbon-Silicon Nanowire Heterostructures for Hydrogen Evolution Reaction

Joonhee Moon,[†,∥,⊥] Uk Sim,[‡,¶,⊥] Dong Jin Kim,[§] Hyo-Yong Ahn,[‡] Junghyun An,[‡] Heonjin Ha,[‡] Kyoung Soon Choi,[∥] Cheolho Jeon,[∥] Jouhahn Lee,[∥] Ki Tae Nam,[‡] and Byung Hee Hong[†,§,]**

[†]Department of Chemistry, Seoul National University, 1 Gwanak-ro Seoul 151-744, Republic of Korea

[∥] Advanced Nano-Surface Research Group, Korea Basic Science Institute, Gwahak-ro, Yuseong-gu, Daejeon 34133, Republic of Korea

[‡]Department of Materials Science & Engineering, Seoul National University, 1 Gwanak-ro Seoul 151-742, Republic of Korea

[¶]Department of Materials Science & Engineering, Chonnam National University, Gwangju 61186, Republic of Korea

[§]Graduate School of Convergence Science and Technology, Seoul National University, Seoul 08826, Republic of Korea

[⊥] These authors contributed equally to this work

Keywords: carbon nanowire (CNW), copper-vapor-assisted chemical vapor depostion, silicon nanowire (SiNWs), hydrogen evolution reaction (HER), metal free catalyst

Figure S1. Growth condition of CNW using CVD system. Each growth-step was controlled by growth time.

Figure S2. Scanning electron microscopy (SEM) image (a) and energy-dispersive X-ray spectroscopy (EDS) maps of (b) carbon, (c) silicon, (d) oxygen in the CNW grown on SiNW electrode.

Figure S3. (a) TEM image of the CNW growth on SiNW in Step 3. The thickness fringes indicate the SiNW etched as a column with angled edges and selective area electron diffraction (SAED) patterns show that (b) p-SiNW was well etched toward [001] direction.

Figure S4. Si $2p_{3/2}$ core-level spectra taken from the CNW-SiNWs surface using X-ray photoelectron spectroscopy (XPS).

Figure S5. Electrochemical activity of bare SiNWs and CNW-SiNWs system. (a) Nyquist plot for bare SiNWs and CNW-SiNWs (Step 3) at 0 V vs. RHE under illumination condition. Inset image is the magnified image near at zero point. (b) Mott-Schottky plots derived from capacitance measurements as a function of potential vs. RHE under dark condition.

Figure S6. The contact angle of de-ionized water droplets on the CNWs-SiNWs substrates for Steps 1 to 4 ((a) to (d)), showing that the angle increases with the as more and longer CNWs are growing on SiNWs.

Figure S7. XPS spectra of (a) the bare SiNWs and (b) CNW-SiNWs (Step 3) before/after the chronoamperometry test at 0 V vs. RHE for 30 hrs, respectively. Narrow-scan data of the Si 2p region were collected using a pass energy of 40 eV and 0.05 eV per step.

Table S1. Summary of experimental data for non-noble metal/metal oxide or carbon-based catalysts on p-Si electrodes.

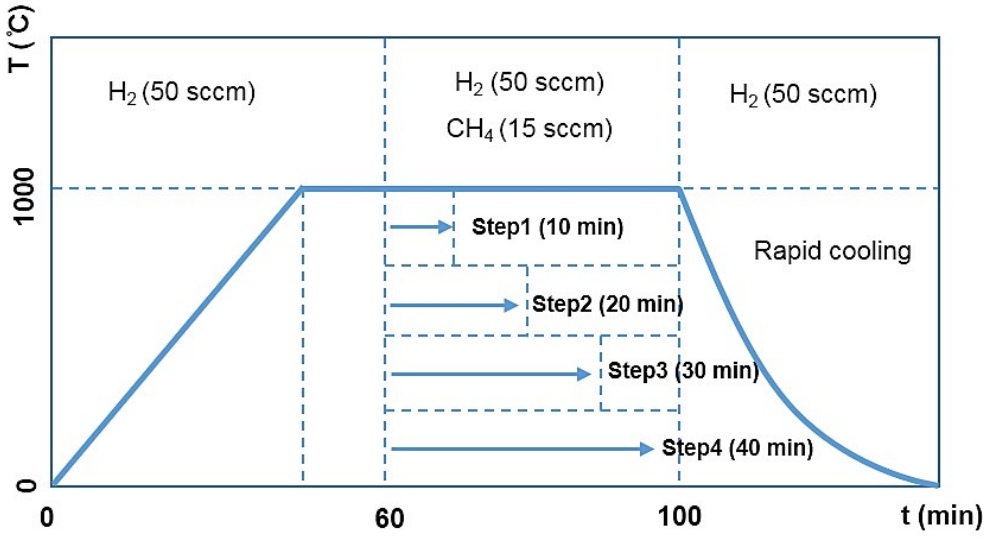

Figure S1. Growth condition of CNW using CVD system. Each growth-step was controlled by growth time.

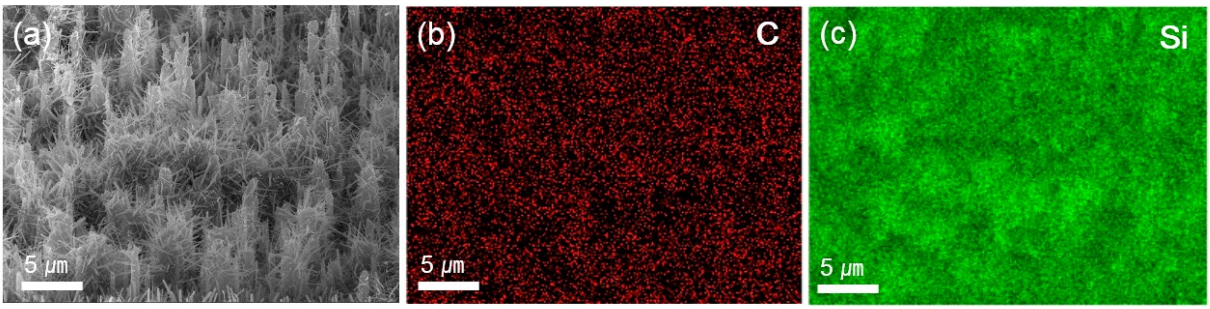

Figure S2. Scanning electron microscopy (SEM) image (a) and energy-dispersive X-ray spectroscopy (EDS) maps of (b) carbon, (c) silicon in the CNW grown on SiNW electrode.

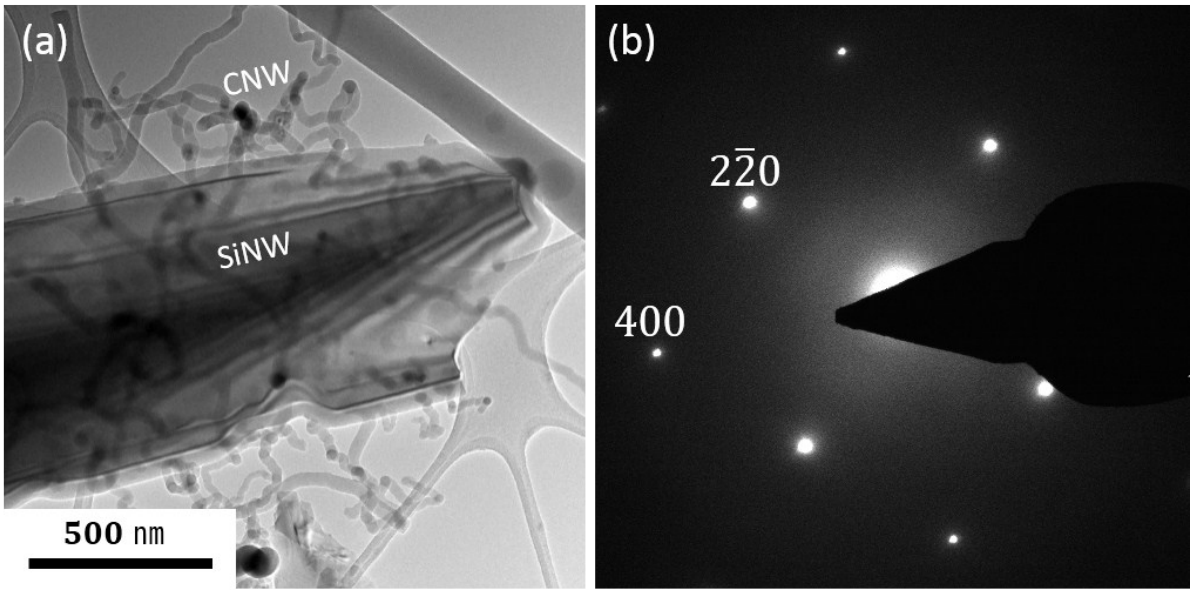

Figure S3. (a) TEM image of the CNW growth on SiNW in Step 3. The thickness fringes indicate the SiNW etched as a column with angled edges and selective area electron diffraction (SAED) patterns show that (b) p-SiNW was well etched toward [001] direction.

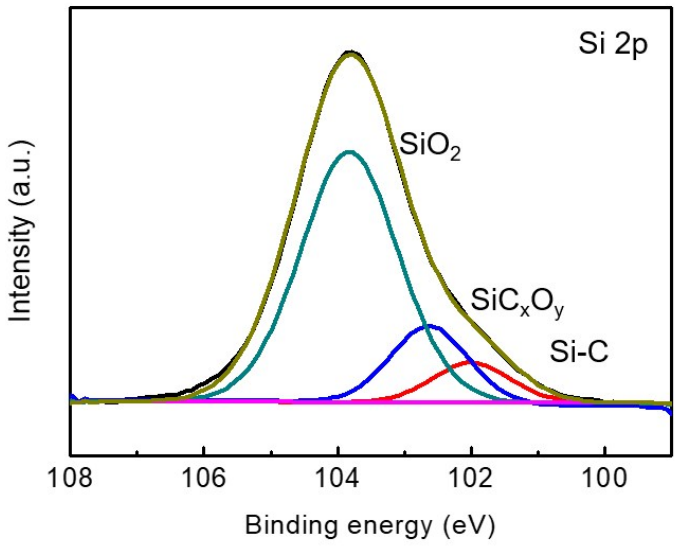

Figure S4. Si $2p_{3/2}$ core-level spectra taken from the CNW-SiNWs surface using X-ray photoelectron spectroscopy (XPS).

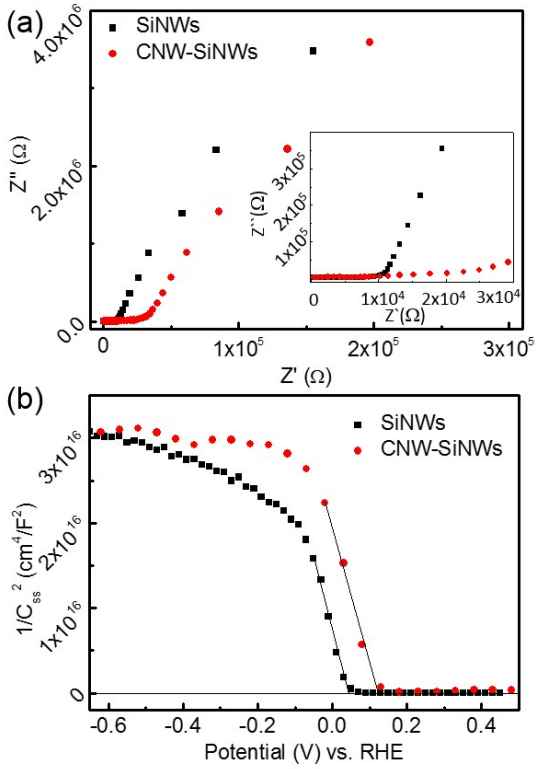

Figure S5. Electrochemical activity of bare SiNWs and CNW-SiNWs system. (a) Nyquist plot for bare SiNWs and CNW-SiNWs (Step 3) at 0 V vs. RHE under illumination condition. Inset image is the magnified image near at zero point. (b) Mott-Schottky plots derived from capacitance measurements as a function of potential vs. RHE under dark condition.

Detailed experimental details for impedance and capacitance measurements and discussion

Impedance and capacitance measurements were also performed to study the electrochemical catalytic properties of the CNW-SiNWs system and it is confirmed that CNW-SiNWs system enhances the hydrogen evolution reaction activity by lowering the kinetic barriers for the HER at the interface between the Si semiconductor and electrolyte solution in terms of reduced charge transfer resistance and enhanced band bending property. Specifically, impedance measurements were performed to study the enhanced electrochemical properties of the CNW-SiNWs system. Electrochemical impedance spectroscopy was performed at 0 V vs. RHE under an illumination intensity of 100 mW/cm^2 with a frequency from 10^6 to 1 Hz and an amplitude of 5 mV. Figure S6 a shows a Nyquist plot representing a typical impedance result. The CNW-SiNWs electrode shows a semicircle that are smaller than those exhibited by the bare SiNWs. On the basis of the results gathered from the semicircle, capacitance elements can be assigned as the capacitance of the charge depletion layer in the semiconductor, or the capacitance of the double layer at the semiconductor/electrolyte interface. In the case of the CNW-SiNW electrodes, the smaller semicircle indicating charge transfer processes in the double layers at the solid/solution interface, or in the depletion region of the semiconductor are smaller than those of the bare SiNWs. The charge transfer resistance is also related to the kinetic barrier energy for the faradaic reactions across the double (D. Merki *et al*, *Chemical Science*, 2012, 3, 2515–2525). Thus, CNWs might promote

the faradaic reactions by reducing the charge transfer resistance across the double layer or in the depletion region. A similar charge transfer mechanism in hydrogen production was also reported using a reduced graphene oxide catalyst (Z. Huang *et al*., *ACS Applied Materials & Interfaces*, 2013, 5, 1961–1966). The charge transfer resistance in the semiconductor depletion layer is also correlated with the higher photocurrent response because of the higher band bending in the depletion layer (N. S. Lewis, *Journal of Electrochemical Society*, 1984, 131, 2496–2503, and T. Lopes *et al*., *International Journal of Hydrogen Energy*, 2010, 35, 11601–11608).

Capacitance measurements of the bare SiNWs and CNW-SiNWs photocathodes were also performed as the potential was swept from 0.5 V to -0.7 V vs. RHE without illumination. On the basis of the capacitance results, the flat band potential of each electrodes was calculated using the Mott–Schottky relationship, $1/C_{sc}^2 = 2(E - E_{fb} - kT/e)/(e\varepsilon\varepsilon_0 N)$ (L. R. F. Allen and J. Bard, *Electrochemical Methods:Fundamentals and Applications*, John Wiley & Sons, Inc., 2001, 864.*)*, where C_{sc} is the capacitance of the space charge region, ε is the dielectric constant of the semiconductor, ε_0 is the permittivity of free space, N is the hole acceptor concentration, E is the applied potential, and E_{fb} is the flat band potential. Figure S6 b shows the typical Mott–Schottky plots for a p-type silicon semiconductor. E_{fb} was determined by extrapolation to a capacitance of zero. On the basis of these relations, the CNW-SiNWs exhibited an E_{fb} of 0.123 V vs. RHE, whereas the E_{fb} of the bare SiNWs was 0.040 V vs. RHE. According to the equation: $E_b = E - E_{fb}$, the applied potential determines the magnitude of band bending (E_b) in the semiconductor and E_{fb} (K. Gelderman *et al.*, *Journal of Chemical Education,* 2007, 84, 685). Higher band bending at the interface between the electrode and electrolyte promotes faster charge separation of generated electrons and holes. The possibility of charge recombination or surface trapping at sub-band gap energy levels may also be diminished. The higher E_{fb} of the CNW-SiNWs electrode relative to that of the bare SiNWs appears to have increased the extent of band bending in the depletion region of the semiconductor near the solid/solution interface because of the relationship between E_b and E_{fb}.

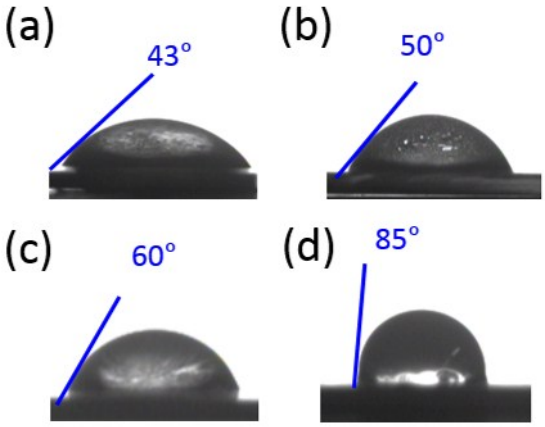

Figure S6. The contact angle of de-ionized water droplets on the CNWs-SiNWs substrates for Steps 1 to 4 ((a) to (d)), showing that the angle increases with the as more and longer CNWs are growing on SiNWs.

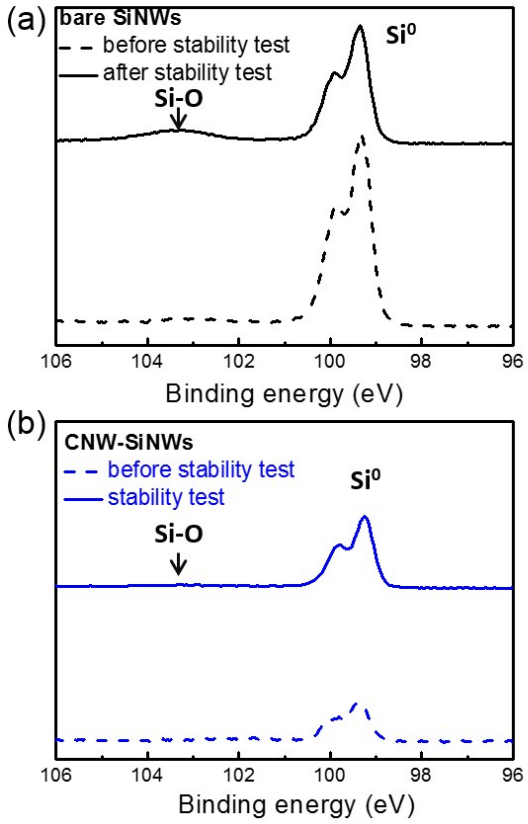

Figure S7. XPS spectra of (a) the bare SiNWs and (b) CNW-SiNWs (Step 3) before/after the chronoamperometry test at 0 V vs. RHE for 30 hrs, respectively. Narrow-scan data of the Si 2p region were collected using a pass energy of 40 eV and 0.05 eV per step.

Table S1. Summary of experimental data for non-noble metal/metal oxide or carbon-based catalysts on p-Si electrodes.

Electrode	Onset potential [E (V_{RHE} at -1 mA/cm^2]	E (V_{RHE}) at -5 mA/cm^2	E (V_{RHE}) at -10 mA/cm^2	ABPE (%)	References
Bare p-si nanowire	**+0.17**	**+0.12**	**+0.09**	**0.91**	***This study***
Carbon seed (step 1) on p-Si nanowire	**+0.23**	**+0.09**	**+0.02**	**0.45**	
Carbon nanowire (step 2) on p-Si nanowire	**+0.33**	**+0.19**	**+0.09**	**1.04**	
Carbon nanowire (step 3) on p-Si nanowire	**+0.37**	**+0.26**	**+0.18**	**1.86**	
Carbon nanowire (step 4) on p-Si nanowire	**+0.24**	**+0.09**	**-0.01**	**0.47**	
Double-layer graphene on p-Si	+0.05	-0.04	-0.11	0.05	*ACS Appl. Mater. Interfaces,* Just Accepted Manuscript, DOI: 10.1021/acsami.6b11750 (Previous results from our group)
Ar plasma-treated double-layer graphene on p-Si	+0.15	0.07	0.01	0.32	
Graphene on p-Si	+0.01	-0.13	-0.21	0.02	*Energy Environ. Sci.,*

N-doped graphene monolayer on p-Si	+0.12	+0.02	-0.04	0.16	2013,**6**, 3658 (Previous results from our group)
N-doped graphene quantum sheets on p-Si nanowire	+0.26	+0.19	+0.16	2.29	*Energy Environ. Sci.,* 2015,**8**, 1329 (Previous results from our group)
$NiCoSe_x$ on p-Si	+0.05	+0.1	-0.08	N/A (~≤0.5)	*Energy Environ. Sci.,* 2016, **9**, 3113
$NiCoSe_x$ on p-Si nanopillar	+0.21	+0.18	+0.16	N/A (~2.3-2.8)	
rGO on p-Si nanowire	-0.1	-0.5	-0.85	N/A (~≤0.05)	*Dalton Trans.,* 2016, **45**, 13717
NiB on p-Si nanowire	+0.43	+0.34	+0.24	2.45	*ACS Appl. Mater. Interfaces,* 2016, **8**, 30143
CoB on p-Si nanowire	+0.44	+0.34	+0.24	2.53	
Bare p-Si	-0.41	-0.55	-0.60	N/A	*Nano Lett.* 2011, **12**, 298
Bare p-Si	-0.35	-0.52	-0.60	N/A	*Energy Environ. Sci.,* 2011,**4**, 1690
Bare p-Si	-0.03	-0.17	N/A (saturated at -9 mA/cm^2)	N/A	*ACS Appl. Mater. Interfaces.* 2013, **5**, 1961
rGO on p-Si	+0.08	-0.05	-0.14	0.005	
rGO on p-Si nanowire	+0.12	-0.04		0.15	
Bare	-0.51	-0.64	-0.77	N/A	*Nat. Mater.* 2011, **10**, 434
Mo_3S_4 on p-Si	+0.12	+0.07	-0.01	~0.2	
Mo_3S_4 on p-Si nanowire	+0.12	+0.08		~0.38	
CuW_3S_4 on p-Si	-0.16	-0.22	-0.29	N/A (~≤0.001)	*J. Photon. Energy* 2012, **2**, 026001
$CuMo_3S_4$ on p-Si	+0.12	+0.06	0.00	~0.2	
W_3S_4 on p-Si	-0.18	-0.25	-0.31	N/A (~≤0.001)	
CoW_3S_4 on p-Si (1st scan)	-0.12	-0.22	-0.3	N/A (~≤0.001)	
$CoMo_3S_4$ on p-Si (1st scan)	-0.02	-0.08	-0.15	N/A (~≤0.001)	
Bare p-Si	-0.50	N/A	N/A	N/A	*Chem. Eur. J.* 2012, **18**, 13994
MoS_2 on p-Si	-0.06	-0.25	-0.35	0.04	
Bare p-Si	-0.25	-0.35	-0.45	N/A	*J. Mater. Chem. A* 2014, **2**, 12697
g-C_3N_4 on p-Si	0	-0.15	-0.25	~0.2	
Bare p-Si	-0.34	-0.47	-0.53	N/A	*Thin Solid Films* 2016, **616**, 550-554
1.4 nm Al_2O_3 on p-Si	-0.21	-0.33	-0.4	N/A (~≤0.001)	
Bare p-Si	-0.05	-0.28	-0.38	N/A	*Nano Res.* 2015, **8**(5), 1577
5 nm Ni/15 nm Ti on p-Si	+0.22	+0.12	0.08	~1.44	
Bare p-Si	-0.7	-0.9	-1.0	N/A	*J. Mater. Chem. A* 2016, **4**, 9477
TiO_2 film/p-Si	-0.4	-0.5	-0.6	N/A	
TiO_2 nanorod/p-Si	-0.05	-0.13	-0.25	N/A (~≤0.002)	
$SrTiO_3$ on p-Si	+0.42	+0.25	+0.01	~1.56	*Nat. Nanotech.* 2015, **10**, 84
WS_2 on p-Si	+0.12	+0.03	-0.04	~0.28	*ACS Appl. Mater. Interfaces.* 2014, **6**, 10408
WS_3 on p-Si	+0.36	+0.27	+0.20	~2	

Values were measured and extrapolated by our group referring to the figures and data from other papers.